Numerical analysis on tensile properties of composite hybrid bonded/bolted joints with flanging

Xiaoquan Cheng [*1], Jie Zhang [1], Jikui Zhang [1], Peng Liu [1], Yujia Cheng [1] and Yahong Xu [2]

[1] *School of Aeronautic Science and Engineering, Beihang University, Beijing 100191, China*
[2] *Institute 306 of the 3rd Academy of CASIC, Beijing, 100074, China*

Abstract. A detailed study was carried out on the tensile properties of the single-lap joint of a steel panel bolted/bonded to a composite laminate with a flanging. Finite element model (FEM) was established to predict the strength and to analyze the damage propagation of the hybrid joints by ABAQUS/Standard, which especially adopted cohesive elements to simulate the interface between the laminate and adhesive. The strength and failure mode predicted by FEM were in good agreement with the experimental results. In addition, three influence factors including adhesive thickness, bolt preload and bolt-hole clearance were studied. The results show that the three parameters have effect on the first drop load of the load-displacement curve, but the effect of bolt-hole clearance is the largest. The bolt-hole clearance should be avoided for hybrid joints.

Keywords: composite structures; hybrid structure; failure mode; damage; finite element method

1. Introduction

Joint design is significant in composite structure design because improper design may lead to defective or conservative structures. Composite laminates are commonly joined with other structures by adhesive bonding, mechanical fastening or combination of these two methods (Marannano and Zuccarello 2015). Among them, bolted joints have high reliability and load transfer capability, and they are easy to disassembly. However, the stress concentration at the holes is severe due to the introduction of the bolts. Compared with bolted joints, bonded joints mainly have the advantages of less stress concentration, none hole damage, less weight increase and so on. However, the load transfer capacity of bonded joints is limited, and the joints are sensitive to the environment and difficult for nondestructive testing. Hybrid joints possess two load transfer paths (bolt and adhesive), which can improve the reliability of the joint structures. With proper design parameter, hybrid joints can combine the advantages of bonded and bolted joints (Chowdhury 2016, Chowdhury *et al*. 2015).

Many researchers have studied hybrid bolted/bonded joints through experimental or numerical methods. Hart-Smith (1982, 1985) studied the static strength of titanium-to-composite hybrid joints using theoretical and experimental approaches. It was found that the strength of the hybrid joints is not improved compared to the corresponding bonded joints, but the damage tolerance of the joints is enhanced and the damage propagation of the adhesive layer is restricted to a certain extent. In addition, it was found that 98% of the load is transferred by adhesive

layer. Kelly (2005) used a 3D finite element model to predict the load sharing in the single-lap hybrid composite joints and then performed experiments to verify the numerical method. The effect of the laminate thickness, adhesive thickness, overlap length, width to diameter ratio (*w/d*) and adhesive modulus on the load sharing ratio of the bolt was studied. His study makes sense for structure design in engineering, but the load-carrying capability of the joints was not analyzed. The static strength and fatigue life of hybrid (bonded/bolted) joints were investigated by Kelly (2006). He experimentally studied the effect of adhesive material properties and laminate stacking sequences on the performances of the joints, and the stress distribution in adhesive layer and the load sharing ratio of the bolt were predicted by finite element analysis (FEA). The hybrid joints prove to have greater static strength, stiffness and fatigue life compared with the bonded joints. The experimental research revealed that the adhesive materials and the stacking sequence have great effect on the properties of composite hybrid joints, though relatively high modulus of the adhesives has no obvious improvement to the strength of the hybrid joints. However, his FEM did not consider the laminate damage, so it cannot give the damage process. Kweon *et al*. (2006) evaluated the strength of composite-to-aluminum double-lap joints, involving adhesive bonded, bolt fastened and hybrid joints with two types of the adhesive (film and paste forms). The results show that for the hybrid joints with the paste adhesive, the strength was higher if the mechanical fastening was stronger than the bondline, while with the film adhesive, the bolt contributes little to the strength of hybrid joints. However, without showing the damage propagation of the hybrid joints, it is still difficult to understand the mechanism of those joints. Lee *et al*. (2010) experimentally investigated the properties of hybrid joints with different

---

*Corresponding author, Ph.D., Professor,
E-mail: xiaoquan_cheng@buaa.edu.cn

width-to-diameter ratios (w/d), edge-to-diameter ratios (e/d) and adherend thicknesses. A high-speed camera was used to capture the crack initiation and propagation of the adhesive layer, while Acoustic Emission (AE) signal was used to capture the AE events and waveforms. The strength of the joints was predicted using Failure Area Index (FAI) and the damage zone method by ANSYS. The relative errors of the numerical ultimate strength kept about 23%. From the load-displacement (L-D) curves and AE signals, the cracks in the adhesive layer occur at the first peak of the L-D curve, but whether the mechanical fastening failure occurs is unknown at this time. Unappropriated damage criteria and evolution laws adopted in their FEM are the reason of relatively high errors. Bois *et al*. (2013) proposed an analytical model for bolted/bonded composite joints. The model included the nonlinear behavior to evaluate precisely the bolt load transfer contribution up to failure. Each expected failure mode was taken into account using a multi-criteria approach which allowed each related criterion to be identified from an elementary (non-hybrid) test. Bodjona *et al*. (Bodjona *et al*. 2015, Bodjona and Lessard 2015) experimentally and numerically explored the load sharing in the single-lap bonded/bolted composite joints and discussed the effect of design parameters on load sharing between the bolt and the adhesive. Results show that the adhesive carries the most of the load and the bolt carries the more load with the more plastic area in the adhesive. And the e/d, adhesive hardening slope and adhesive yield strength have great effect, while the adhesive thickness and bolt-hole clearance have relatively less effect compared with the former three parameters. The adhesive elastic-plastic behavior was considered in the model with ignorance of the joint damage, so damage mechanism was not investigated. Most of the researches have taken the plate as their objects until now.

In this paper, a hybrid bonded/bolted joint with a flanging was studied. The joint consists of composite laminate and steel panel, which is from an engineering structure. A flanging was designed due to the limitation of the edge distance of the composite part. Tensile experiment of single-lap hybrid joints with three specimens was conducted, and a FEM was established to predict the tensile strength of the joint and to simulate the damage propagation, which mainly focused on the damage of the composite laminate, adhesive layer and interfaces between the adhesive and adherends. The FEM was validated by experimental results in the aspects of ultimate strength and failure mode. With the validated model, the damage mechanism was analyzed in detail and three influencing factors, including the adhesive thickness, bolt preload and bolt-hole clearance, were investigated. The investigation results can provide a reference for the design of short-edge-distance hybrid composite joints.
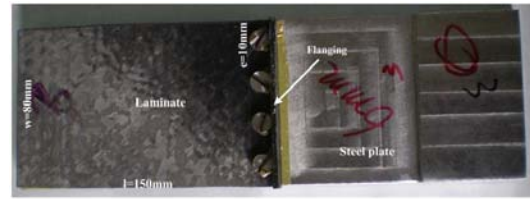
Fig. 1 The specimen and its geometry

2. Specimen configuration

The specimens used for the experiment here are from an engineering structure. A composite laminate is joined with a steel panel through 4 bolts and an adhesive layer, and the specimen geometry is shown in Fig. 1. A flanging at the end of the laminate was designed because of the space limitation. The laminate was fabricated by Resin Transfer Molding (RTM) process. Then, a layer of adhesive of J-47 was placed between the steel panel and laminate and cured at 130 degree centigrade for 2h. Four holes were drilled by peck feed drilling, and then four bolts were installed with the bolt torque of 1.5 N·m.

The material of laminate is 3327/6808 (carbon fiber plain woven ply/epoxy) with ply sequence $[(\pm45)/(0, 90)]_{3S}$ and the thickness of each ply is 0.28 mm. The properties of 3227/6808 ply are shown in Table 1. The metal panel and bolts are made of steel 30CrMnSi with the Young's modulus of 196 GPa and Poisson ratio of 0.3. The plasticity of the steel is also considered. The yield strength is 1105 MPa, and the slope of stress-strain becomes zero after the steel yields. J-47 is a brittle adhesive with the Young's modulus of 3 GPa, shear strength of 30 MPa, Poisson ratio of 0.3 and the nominal thickness of 0.1 mm.

3. Finite element model

3.1 Model details

It was assumed that four bolts had the same joining condition, i.e. each bolt carried the same load. To simplify the model and save solving time, one eighth of the joint was

Table 1 Properties of 3327/6808 ply

Properties	E_{11} (GPa)	E_{22} (GPa)	E_{33} (GPa)	G_{12} (GPa)	v_{12}	v_{13}	v_{23}
Values	75	74.2	8	3.5	0.06	0.31	0.31
Properties	X_t (MPa)	X_c (MPa)	Y_t (MPa)	Y_c (MPa)	S_{12} (MPa)	S_{13} (MPa)	S_{23} (MPa)
Values	750	550	750	550	70	70	70

The contacts of the bolt/laminate and the bolt/steel panel were considered, and surface-to-surface contact was implemented on four contact pairs and the master-slave relationship was the same with Liu *et al.* (2016). A friction coefficient of 0.3 was applied to all the contact pairs. The bolt preload corresponding to the bolt torque of $1.5\text{N}\cdot\text{m}$ was 1 kN (Nuismer and Whitney 1975, Wang *et al.* 2016). The bolt-hole clearance was zero.

3.2 Failure criteria and damage evolution for composite laminate

For plain fabric composite laminate, classified damage criteria (Xiao and Takashi 2005, Kallmeyer and Stephen 1999, Reifsnider and Case 2000, Aghaei *et al.* 2015) were adopted to predict damage initiation. The expressions of the criteria are shown in Table 2.

In Table 2, σ_{11} and σ_{22} represent longitudinal and transversal normal stress. τ_{12}, τ_{13} and τ_{23} represent shear stress. X_T and X_C represent longitudinal tensile and compressive strengths. Y_T and Y_C are transversal tensile and compressive strengths respectively. Z_T and Z_C are normal tensile and compressive strengths. S_{12}, S_{13} and S_{23} stand for in-plane and interlaminar shear strengths.

The stiffness degradation rules adopted in the model are also shown in Table 2, which is based on Reddy *et al.* (1993). Once failure is predicted in an element, its material properties are modified with the degradation rules.

3.3 Failure criteria and damage evolution for the adhesive and interfaces

The adhesive used in the experiment is brittle, and

Fig. 2 Finite element model and boundary conditions of the hybrid joint

modeled as shown in Fig. 2. The laminate, steel panel and adhesive layer were modeled as a whole part, and the adhesive is distinguished through the partition operation. 8-node reduced integration solid elements (C3D8R) were chosen for the whole part and 12 elements were used in the through-thickness of the laminate. Two layers of zero-thickness cohesive elements (COH3D8) were applied in the interfaces to simulate the interface damage of the adhesive/laminate and the adhesive/metal panel. The boundary conditions are also shown in Fig. 2. The end face of the steel panel was fixed, symmetric boundary condition was applied on the symmetry plane and the tensile load was applied by displacement on the other end of the specimen.

Table 2 Failure criteria and degradation rules of plain fabric composite

Failure modes	Failure Criteria	Degradation rules
Fiber-matrix shear-out	$\left(\dfrac{\sigma_{11}}{X_C}\right)^2 + \left(\dfrac{\tau_{12}}{S_{12}}\right)^2 + \left(\dfrac{\tau_{13}}{S_{13}}\right)^2 \geq 1$	$G_{12} = 0.2G_{12},$ $v_{12} = 0.2v_{12},$
Weft fiber tensile failure $(\sigma_{22} \geq 0)$	$\left(\dfrac{\sigma_{22}}{Y_T}\right)^2 + \left(\dfrac{\tau_{12}}{S_{12}}\right)^2 + \left(\dfrac{\tau_{23}}{S_{23}}\right)^2 \geq 1$	$E_{22} = 0.07E_{22},\ E_{33} = 0.2E_{33},$ $G_{12} = 0.07G_{12},\ G_{23} = 0.07G_{23},$
Weft fiber compressive failure $(\sigma_{22} \leq 0)$	$\left(\dfrac{\sigma_{22}}{Y_C}\right)^2 \geq 1$	$v_{12} = 0.07v_{12},\ v_{23} = 0.07v_{23}$
Tensile delamination $(\sigma_{33} \geq 0)$	$\left(\dfrac{\sigma_{33}}{Z_T}\right)^2 + \left(\dfrac{\tau_{23}}{S_{23}}\right)^2 + \left(\dfrac{\tau_{13}}{S_{13}}\right)^2 \geq 1$	$E_{33} = 0.01E_{33},$ $G_{12} = 0.01G_{12},\ G_{13} = 0.01G_{13},$
Compressive delamination $(\sigma_{33} \leq 0)$	$\left(\dfrac{\sigma_{33}}{Z_C}\right)^2 + \left(\dfrac{\tau_{23}}{S_{23}}\right)^2 + \left(\dfrac{\tau_{13}}{S_{13}}\right)^2 \geq 1$	$v_{23} = 0.01v_{23},\ v_{13} = 0.01v_{13}$
Warp fiber tensile failure $(\sigma_{11} \geq 0)$	$\left(\dfrac{\sigma_{11}}{X_T}\right)^2 + \left(\dfrac{\tau_{12}}{S_{12}}\right)^2 + \left(\dfrac{\tau_{13}}{S_{13}}\right)^2 \geq 1$	$E_{33} = 0.01E_{33},$ $G_{12} = 0.01G_{12},\ G_{13} = 0.01G_{13},$
Warp fiber compressive failure $(\sigma_{11} \leq 0)$	$\left(\dfrac{\sigma_{11}}{X_C}\right)^2 \geq 1$	$v_{23} = 0.01v_{23},\ v_{13} = 0.01v_{13}$

maximum shear stress criterion was chosen to predict the initial damage of the adhesive. The criterion is as follows

$$\tau_{\max} = (\sigma_{11} - \sigma_{33})/2 \geq [\tau] \tag{1}$$

Once $\tau_{\max}$ reached the shear strength of the adhesive, the adhesive would fail and the properties of adhesive would degrade as: $E_a = 0.01E_a$, $v = 0.01v$.

As mentioned before, cohesive elements were used to simulate the interfaces between the adhesive and adherends. The progressive damage and failure of cohesive layers were modeled using traction-separation law. The interface stiffness of the cohesive element was the same as Liu *et al.* (2016). The quadratic nominal stress criterion was chosen as damage initiation criterion for cohesive elements. The criterion can be given as below

$$\left(\frac{\langle t_n \rangle}{t_n^0}\right)^2 + \left(\frac{t_s}{t_s^0}\right)^2 + \left(\frac{t_t}{t_t^0}\right)^2 = 1 \tag{2}$$

Where t_n, t_s and t_t represent the stresses that are normal to the interface, in the first shear direction and in the second shear direction, respectively. t_n^o, t_s^o and t_t^o represent normal strength, the first shear strength and the second shear strength of cohesive elements respectively and the corresponding values are 60 MPa, 40 MPa and 40 MPa. It is noted that the Macaulay bracket was used to signify that a pure compressive stress state does not initiate damage.

The damage evolution law based on the energy was used for cohesive elements. The energy is dissipated when the damage expands and it is equal to the area OAB under the traction-separation curve (see Fig. 3) (Kharazan *et al.* 2014). The linear softening behavior was assumed. The mixed mode of deformation fields in the cohesive zone was utilized. Benzeggagh-Kenane (BK) fracture criterion (Abaqus-Inc. 2012) was adopted in which the critical fracture energies during deformation purely along the first and the second shear directions are the same; i.e., $G_s^C = G_t^C$. BK criterion is given by

$$G_n^C + (G_s^C - G_n^C)\{\frac{G_S}{G_T}\}^\eta = G_{TC} \tag{3}$$

where $G_S = G_s + G_t$, $G_T = G_n + G_S$, and G_n, G_s and G_t are
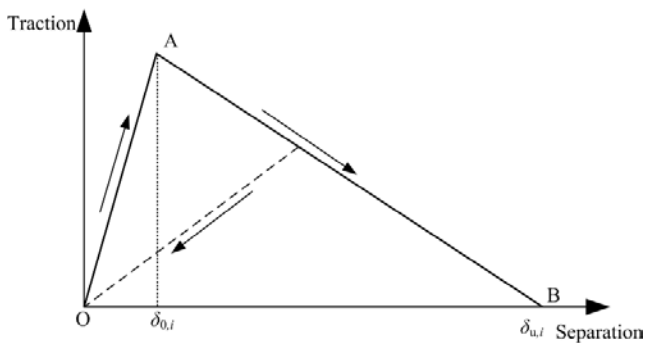
dissipated energies per unit area of Mode I, II and III. G_n^C, G_s^C and G_t^C are energy release rates of Mode I, II and III, and the values are 1.2 N/mm, 2.5 N/mm and 2.5 N/mm respectively. η is a material parameter which is 1.5 in the model. G_{TC} is the mixed-mode energy release rates and is calculated by Abaqus based on G_n^C, G_s^C and G_t^C. The cohesive viscosity coefficient of 0.001was used to improve the model convergence.

4. Results and discussion

Experimental and numerical results show that the steel panels and bolts were still in the elastic state, thus their properties were not analyzed in the following sections.

4.1. Load-displacement curve

Fig. 4 shows the load-displacement curve of FEA, and the comparison of numerical and experimental results is shown in Table 3. From Fig. 4, it can be seen that there are four characteristic points (A, B, C and D) on the curve. Before Point A, the load-displacement curve is almost linear and the stiffness is a little bit degraded after Point A due to the fiber breakage close to the free end of the steel panel. That is because the stiffness of the joint structure has a big change at this damage area. Afterwards, an obvious drop appears at Point B (about 30 kN) due to the damage expansion of the adhesive layer. At this time, cracking noise was heard in the experiment. At Point C, the damage in the joint is severe, thus bolt sharing ratio is large. The joint reaches its ultimate strength at Point D.

The joint finally fails at Point C, and ultimate failure modes of the experiment and FEM are shown in Fig. 5. All the specimens fail with net-section mode, and the numerical result also shows the similar failure profile with lots of fiber breakage throughout the section. Obvious delamination can be found at the bending position of flanging in both tests and FEM due to the bearing stress around the hole, the short edge distance and flanging. The FEM results show that extra delamination occurs at the place close to the free end of the steel panel, which is caused by peeling stress from bending load of the laminate. Therefore, the model was

Fig. 3 Typical traction-separation response and linear damage evolution of cohesive elements
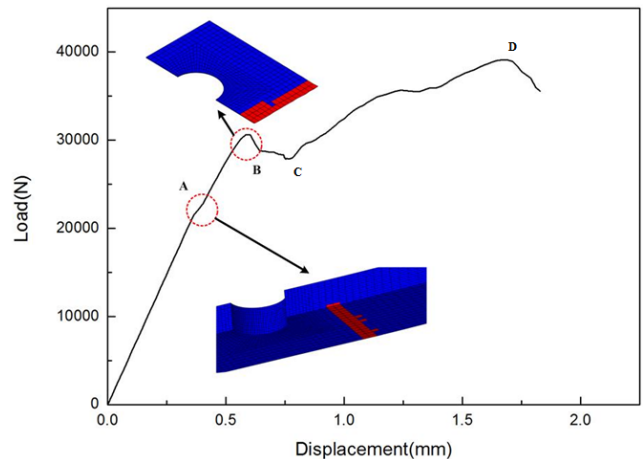

Fig. 4 Load-displacement curve of FEA
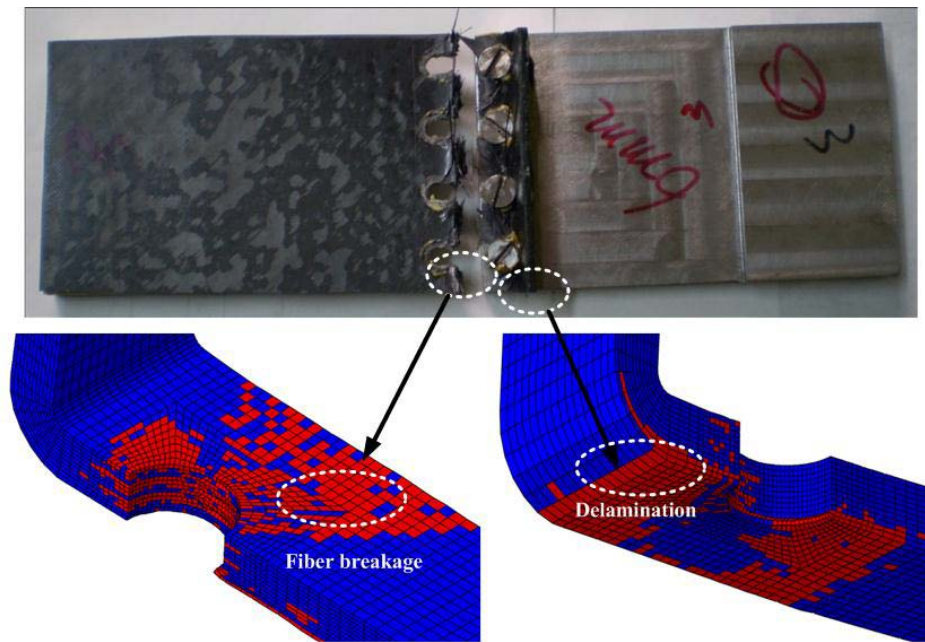
Fig. 5 Failure profiles of the Experiment and FEM

Table 3 Comparisons of experimental and numerical results in terms of failure loads and damage phenomena
(*w* = width, *h* = height, *t* = thickness)

Specimen number or FEM	Laminate w×t (mm×mm)	Flanging h×t (mm×mm)	Steel panel w×t (mm×mm)	Failure load (kN)	Damage phenomenon
HJ-1	80.92×3.37	12.78×4.23	81.95×8.02	40.86	Cracking noise at 20 kN, obvious delamination at the bending position of flanging, net-section failure
HJ-2	81.26×3.13	13.06×3.95	81.91×8.12	45.08	Cracking noise at 22 kN, obvious delamination at the bending position of flanging, net-section failure.
HJ-3	81.85×3.40	12.84×3.74	82.05×8.05	41.98	Severe cracking noise at 30 kN, obvious delamination at the bending position of flanging, net-section failure.
FEM	80×3	12×3	80×8	39.21	Fiber breakage initiated at 21.55 kN, first load peak at 30.70 kN, obvious delamination at the bending position of flanging, net-section failure

thought to be accurate in the damage prediction.

From Table 3, the average failure load of three specimens is 42.64 kN, while the failure load of FEM is 39.21 kN with a relative error of 8.04%. Thus, the FEM provides acceptable accuracy in predicting the failure load.

4.2 Damage propagation

Fig. 6 shows the damage propagation of the adhesive and interfaces. The initial damage in the adhesive appears close to the free edge of the steel panel at the load of 22.8 kN, which happens just after Point A (see Fig. 4). Meanwhile, the interface damage initiates at the same position both in upper and lower interfaces. The adhesive damage extends in the longitudinal direction in the process of load increase to 30.1 kN, and the damage area of the upper interface is larger than that of the lower interface. At this load, the load-displacement curve appears a drop and

the bolt load is increasing. After that drop, the adhesive damage occurs at the hole. The damage in the upper interface propagates to the hole, and some damage appears at the other end of the lower interface. When the load rebounds to 35 kN, more damage appears around the hole, and the adhesive damage area has reached half the adhesive area. And the upper interface damage appears in the other end, and its area is smaller than the lower's. The adhesive damage propagation stops at 36.8 kN just before the joint failure with some undamaged area, which means that the bolt can restrict the adhesive damage to a certain extent. However, the interface damage continues to propagate in both interfaces. When the joint fails, the damage at the other end is larger in the interfaces but none in the adhesive.

The main damage modes of the composite laminate are weft and warp fiber breakage and delamination. The damage propagating process of the weft fiber breakage is shown in Fig. 7, and the warp fiber breakage is similar. The
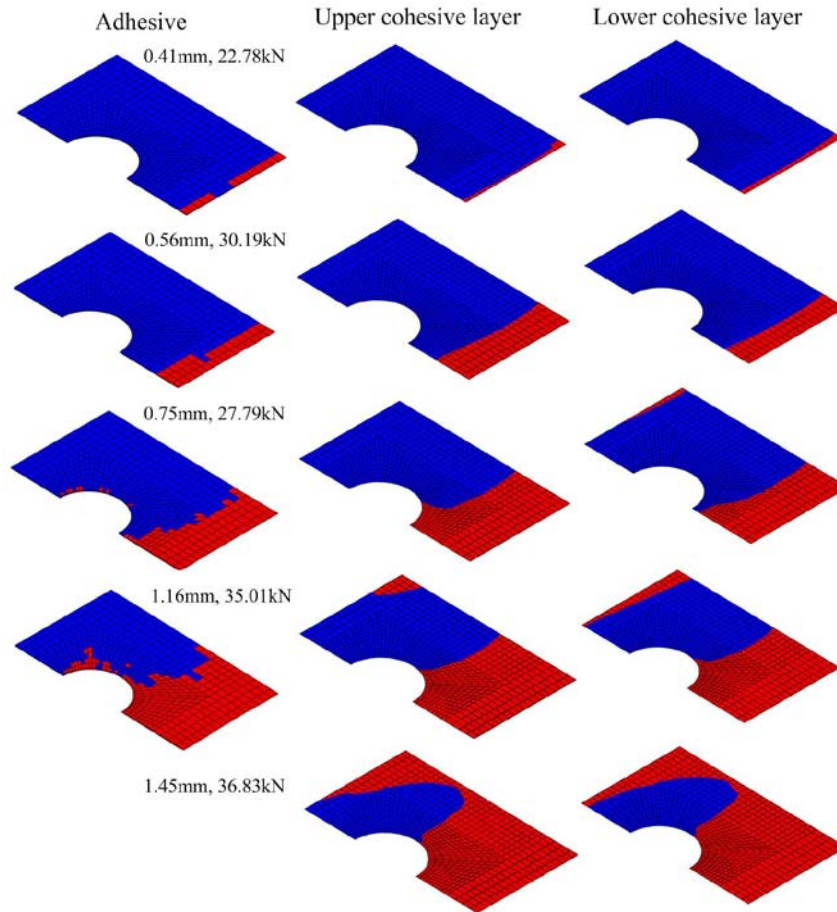
Fig. 6 Damage propagation of the adhesive and interfaces
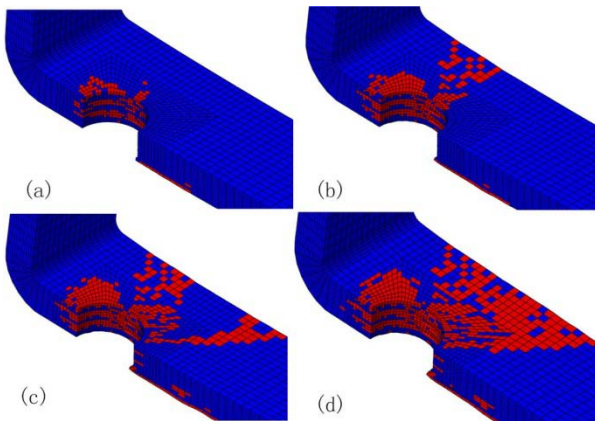
Fig. 7 Weft fiber breakage propagation of the laminate:
(a) 30.08 kN; (b) 35.19 kN; (c) 36.17 kN;
(d) 39.05 kN

weft fiber breakage initiates at the place close to the free end of the steel panel at 22.5 kN, which corresponds to Point A in Fig. 4. When the load reaches 30.08 kN, the damage propagates to the hole, and the hole edge occurs damage at the bearing side. The bolt carries more loads, which leads to faster damage propagating rate at the hole edge and net-section of the composite laminate. With the load increasing, the damage quickly propagates to failure in net section in the region of $\pm 45^{\circ}$ (surface fiber direction).

5. Analysis of influencing factors

5.1 Effect of adhesive thickness

The origin thickness of the adhesive is 0.1 mm, and two more thicknesses of 0.2 mm and 0.3 mm were investigated to study its effect on tensile property of the hybrid joint. The load-displacement curves of three conditions are shown in Fig. 8. The stiffness of three curves is almost the same in initial linear period. It can be seen that the initial damage in the laminate firstly appears in the 0.1 mm thickness case, and then 0.2 mm thickness and 0.3 mm thickness cases sequentially. Therefore, the increase of adhesive thickness can delay the initial damage in the laminate. However, the first obvious load drop occurs earlier for the 0.2 mm and 0.3 mm thickness cases, which is because for larger adhesive thickness, the eccentric moment is greater and the laminate damage at Point A is more serious. After Point C, the load is mainly carried by the bolt, so their curves are close and the failure load seems unaffected by the adhesive thickness.

5.2 Effect of bolt preload

Except 1 kN, two more preloads of 0 kN and 2 kN were chosen to investigate the effect of bolt preload on the tensile property of the hybrid joint. From Fig. 9, the preload has little effect on the initial stage of the load-displacement curves. And compared with the case of 1 kN preload, the
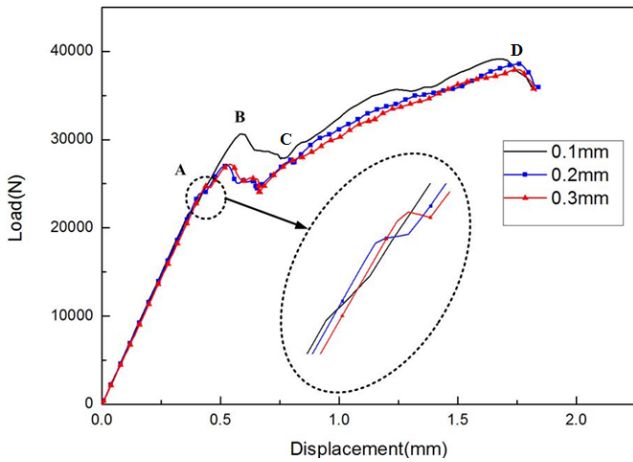
Fig. 8 Load-displacement curves with different adhesive
thicknesses
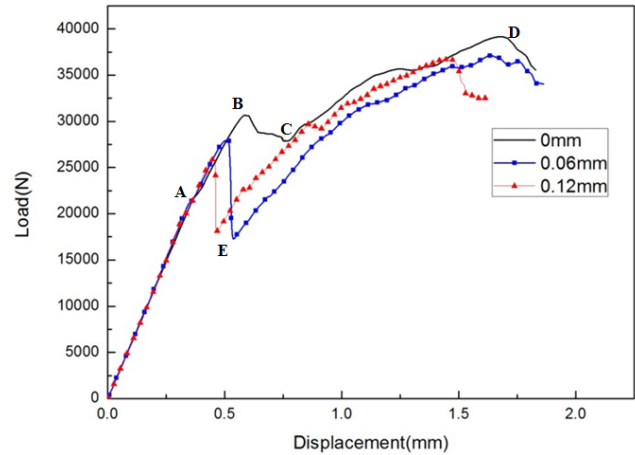
Fig. 10 Load-displacement curves with different bolt-
hole clearances
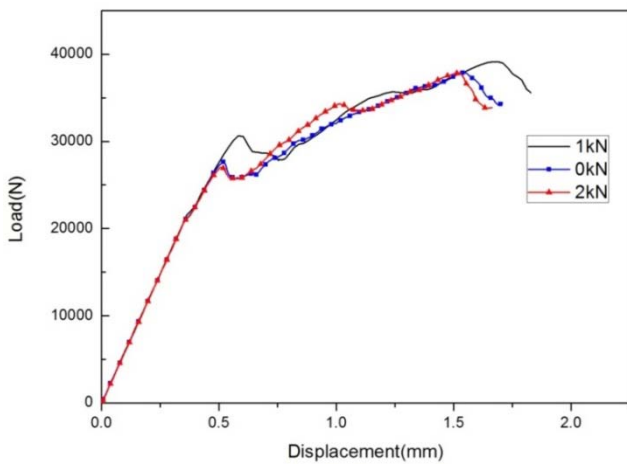
Fig. 9 Load-displacement curves with different bolt
preloads

first load drops appear earlier and failure loads are lower for the cases of 0 kN and 2 kN preloads, which is because appropriate bolt preload can efficiently delay the adhesive damage and prevent the delamination of the laminate and interfaces, but greater preload (2 kN) can cause premature damage in the adhesive and laminate.

5.3 Effect of bolt-hole clearance

Bolt-hole clearance has a significant effect on the properties of the bolted joints (Fan *et al*. 2015), and it may also influence the tensile property and damage propagation of hybrid joints.

The hybrid joints with bolt-hole clearances of 0.06 mm and 0.12 mm (for 1% and 2% bolt diameter respectively) were investigated, and their results were compared with the bolt-hole clearance of 0 mm to analyze the effect of bolt-hole clearance, as shown in Fig. 10. The appearance of bolt-hole clearance leads to greater load decrease at the first drop. For the cases of bolt-hole clearance larger than zero, most loads are carried by the adhesive in initial periods, and larger bolt-hole clearance causes smaller adhesive area, thus

the increase of bolt-hole clearance leads to the decrease of the load at the first drop (Point B). When the hole edge contacts with the bolt, the bolt will carry most of the load, so the values of the loads at Point E are close. At Point D, almost all the regions of the adhesive and interfaces fails for the cases with bolt-hole clearance, and the load is carried only the bolt, thus the failure loads of the two case are similar and less than that of zero-clearance joint. Therefore, the clearance is more significant for the hybrid joint than for the bolted joint, and the clearance should be avoided during the assembly of the hybrid joint.

6. Conclusions

A 3D FEM considering the interface damage was developed to investigate the tensile properties of a special hybrid joint. The model was verified by experimental results in terms of the damage initiation, failure load and ultimate failure mode. The influence of three parameters was studied including the adhesive thickness, bolt preload and bolt-hole clearance. The following conclusions can be obtained:

- The failure load of FEM has a small relative error compared with the experimental results, which proves the validity of the model. The numerical results show the fiber breakage initiates at the place close to the free end of the steel panel. The first load drop corresponds to relatively large damage in the joint. And then, the bolt carries much more load. The failure mode is net-section tensile failure. The steel parts have no damage.
- Increasing adhesive thickness can delay the initial damage in the laminate, the joint damage is more severe and the bolt carries more loads, and the failure load keeps unaffected by the adhesive thickness. Improper tightening torque might exacerbate the joint damage and reduce the failure load of hybrid joint.
- The bolt-hole clearance is more significant for the hybrid joint than for the bolted joint. When the hole

edge contacts with the bolt, the bolt will carry most of the load, and the failure load with clearance is slightly less than that with zero clearance. The bolt-hole clearance should be avoided for hybrid joints.

In the future work, more detailed experiment investigations should be conducted with different kinds of the adhesive, and load sharing between the bolt and adhesive should be investigated by both numerical and experimental methods. In addition, the hygrothermal environmental factors should be considered in the parameter studies.

References

Abaqus-Inc. (2012), Abaqus User Manual, Version 6.11; Dassault Systemes Simulia Corp., Paris, France.

Aghaei, M., Forouzan, M.R., Nikforouz, M. and Shahabi, E. (2015), "A study on different failure criteria to predict damage in glass/polyester composite beams under low velocity impact", *Steel Compos. Struct., Int. J.*, **18**(5), 1291-1303.

Bodjona, K. and Lessard, L. (2015), "Load sharing in single-lap bonded/bolted composite joints. Part II: Global sensitivity analysis", *Compos. Struct.*, **129**, 276-283.

Bodjona, K., Raju, K., Lim, G.H. and Lessard, L. (2015), "Load sharing in single-lap bonded/bolted composite joints. Part I: Model development and validation", *Compos. Struct.*, **129**, 268-275.

Bois, C., Wargnier, H., Wahl, J.C. and Goff, E.L. (2013), "An analytical model for the strength prediction of hybrid (bolted/bonded) composite joints", *Compos. Struct.*, **97**, 252-260.

Chowdhury, N. (2016), "Static and fatigue testing bolted, bonded and hybrid step lap joints of thick carbon fibre/epoxy laminates used on aircraft structures", *Compos. Struct.*, **142**, 96-106.

Chowdhury, N., Chiu, W.K., Wang, J. and Chang, P. (2015), "Static and fatigue testing thin riveted, bonded and hybrid carbon fiber double lap joints used in aircraft structures", *Compos. Struct.*, **121**, 315-323.

Fan, J.F., Cheng, X.Q., Wang, S.W., Guo, X. and Zhang, T. (2015), "Experimental and numerical investigation of composite bolted pi-joint subjected to bending load", *Compos. Part B: Eng.*, **78**, 324-330.

Hart-Smith, L.J. (1982), "Design methodology for bonded-bolted composite joints", Report No. AFWAL-TR-81-3154; Douglas Aircraft Company, CA, USA.

Hart-Smith, L.J. (1985), "Bonded-bolted composite joints", *J. Aircraft*, **22**(11), 993-1000.

Kallmeyer, A.R. and Stephen, R.I. (1999), "Finite element model for predicting time-dependent deformations and damage accumulation in laminated composite bolted joints", *J. Compos. Mater.*, **33**(9), 794-826.

Kelly, G. (2005), "Load transfer in hybrid (bonded/bolted) composite single-lap joints", *Compos. Struct.*, **69**(1), 35-43

Kelly, G. (2006), "Quasi-static strength and fatigue life of hybrid (bonded/bolted) composite single-lap joints", *Compos. Struct.*, **72**(1), 110-129

Kharazan, M., Sadr, M.H. and Kiani, M. (2014), "Delamination growth analysis in composite laminates subjected to low velocity impact", *Steel Compos. Struct., Int. J.*, **17**(4), 307-403.

Kweon, J.H., Jung, J.W., Kim, T.H. and Choi, J.H. (2006), "Failure of carbon composite-to-aluminum joints with combined mechanical fastening and adhesive bonding", *Compos. Struct.*, **75**(1-4), 192-198.

Lee, Y.H., Lim, D.W., Choi, J.H. and Kweon, J.H. (2010), "Failure load evaluation and prediction of hybrid composite double lap

joints", *Compos. Struct.*, **92**(12), 2916-2926.

Liu, P., Cheng, X.Q., Wang, S.W., Liu, S.F. and Cheng, Y.J. (2016), "Numerical analysis of bearing failure in countersunk composite joints using 3D explicit simulation method", *Compos. Struct.*, **138**, 30-39.

Liu, S.F., Cheng, X.Q., Zhang, Q., Zhang, J., Bao, J.W. and Guo, X. (2016), "An investigation of hygrothermal effects on adhesive materials and double lap shear joints of CFRP composite laminates", *Compos. Part B: Eng.*, **91**, 431-440.

Marannano, G. and Zuccarello, B. (2015), "Numerical experimental analysis of hybrid double lap aluminum-CFRP joints", *Compos. Part B: Eng.*, **71**, 28-39.

Nuismer, R.J. and Whitney, J.M. (1975), "Uniaxial failure of composite laminates containing stress concentration", ASTM STP 593.

Reddy, Y.S. and Reddy, J.N. (1993), "Three-Dimensional Finite Element Progressive Failure Analysis of Composite Laminates under Axial Extension", *Compos. Technol. Res.*, **15**(2), 73-87.

Reifsnider, K. and Case, S. (2000), "The mechanics of composite strength evolution", *Compos. Sci. Technol.*, **60**(12-13), 2539-2546.

Wang, S.W., Cheng, X.Q., Guo, X., Li, X. and Chen, G. (2016), "Influence of lateral displacement of the grip on single lap composite-to-aluminum bolted joints", *Exp. Mech.*, **56**(3), 407-417.

Xiao, Y. and Takashi, I. (2005), "Bearing strength and failure behavior of bolted composite joints (part II: modeling and simulation)", *Compos. Sci. Technol.*, **65**(7-8), 1032-1043.

CC